ISSN 0022-4766, Journal of Structural Chemistry, 2021, Vol. 62, No. 5, pp. 771-781. © Pleiades Publishing, Ltd., 2021.
Russian Text © The Author(s), 2021, published in Zhurnal Strukturnoi Khimii, 2021, Vol. 62, No. 5, pp. 827-838.

EFFECT OF STRUCTURE AND SURFACE STATE OF NITROGEN DOPED CARBON NANOTUBES ON THEIR FUNCTIONAL AND CATALYTIC PROPERTIES

O. Yu. Podyacheva[1,2]*, A. N. Suboch[2], S. A. Yashnik[1,2], A. V. Salnikov[1,2], S. V. Cherepanova[2], L. S. Kibis[2], G. Yu. Simenyuk[1], A. I. Romanenko[3], and Z. R. Ismagilov[1,2]

A comprehensive study of nitrogen doped carbon nanotubes (N–CNTs) with nitrogen content varying from 0 at.% to 7.3 at.% is reported. A correlation is revealed between the content of pyridine-like nitrogen and the defectivity of the N–CNT bamboo-like structure. A model of graphene layer with defects containing ordered carbon vacancies and pyridine nitrogen is proposed. The model is based on a combination of experimental data obtained by powder X-ray diffraction, X-ray photoelectron spectroscopy, Raman spectroscopy, scanning electron microscopy and simulation of the N–CNT structure by the use of g-C_3N_4 structural elements. It is shown that more than a two-fold increase of the N–CNT specific capacity in acidic and alkaline electrolytes compared to that of undoped carbon nanotubes is due to the fact that N–CNTs posses significantly better hydrophilic properties due to the defects based on pyridine-like nitrogen centers. The N–CNT efficiency as a catalyst and a palladium catalyst support in the reaction of oxidative desulfurization of dibenzothiophene is demonstrated.

DOI: 10.1134/S0022476621050139

Keywords: carbon nanotubes, doping, nitrogen, structure, defects, specific capacity, catalysts, oxidative desulfurization of dibenzothiophene.

INTRODUCTION

Nitrogen doped carbon nanomaterials (N–CNMs) are currently a subject of rapidly developing research. To date, almost all known nitrogen-containing carbon materials have been successfully synthesized (nanotubes, nanofibers, graphene, various types of porous carbon, nano-onions, spheres, etc.) [1]. Such materials are promising for the use as electrodes of electrochemical devices, adsorbents, catalysts and catalyst supports in various reactions and in electrocatalysis; extensive data are obtained on N–CNM activity in the reactions of oxidation, dehydrogenation, hydrochlorination, aldehyde and ketone condensation, etc. [2]. In turn, metals supported on these materials exhibit higher activity in reactions of selective

[1]Federal Research Center of Coal and Coal-Chemistry, Siberian Branch, Russian Academy of Sciences, Kemerovo, Russia. [2]Boreskov Institute of Catalysis, Siberian Branch, Russian Academy of Sciences, Novosibirsk, Russia; *pod@catalysis.ru. [3]Nikolaev Institute of Inorganic Chemistry, Siberian Branch, Russian Academy of Sciences, Novosibirsk, Russia. Original article submitted October 14, 2020; revised December 15, 2020; accepted December 17, 2020.

hydrogenation, dehydrogenation, oxidation, etc., than metals supported on undoped analogs [3]. Recently, the interest to these objects has increased significantly due to the reported data on the possibility of the preparation of metal catalysts with atomic dispersion by the use of N-CNMs. Two scenarios are possible: the catalyst contains simultaneously nanoparticles and isolated atoms [4] or the catalyst consists of isolated atoms only [5].

The electronic structure of carbon nanomaterials changes as a result of nitrogen doping so that electron transfer in the system may be facilitated or its electron density may undergo local changes [2]. The incorporation of nitrogen into the carbon structure is accompanied by the formation of positive and negative charges on the surface to affect adsorption of reagents and stabilization of supported metals [6]. Also, various structural defects formed in N–CNM graphene layers decrease the size of defect-free graphene blocks [7, 8]. All the above phenomena should determine functional properties of N–CNMs in various applications.

In this work, a comprehensive study of nitrogen doped carbon nanotubes (N–CNTs) is performed to determine how their structure and surface composition affect functional properties of N–CNTs when used as supercapacitor electrodes, catalysts, and palladium catalyst supports in the reaction of oxidative desulfurization of dibenzothiophene.

EXPERIMENTAL

The CNTs and N–CNTs were prepared by decomposing C_2H_4 or C_2H_4/NH_3 ([NH_3] = 25 vol.%, 40 vol.%, 60 vol.%, and 75 vol.%) on catalyst 62%Fe–8%Ni–30%Al_2O_3 at 650-750 °C in a flow-type reactor with a vibro-fluidized catalyst bed. The resulting CNTs and N–CNTs were washed from the growth catalyst in concentrated hydrochloric acid at room temperature and by boiling in 2M HCl for 6 h. Then the samples were washed from chlorine ions by repeated boiling in distilled water until no positive control was registered after adding $AgNO_3$ to the rinsing water. The washed samples were dried in Ar at 170 °C for 2 h. The texture characteristics of CNTs and N–CNTs (S_{BET}, m^2/g) were studied by low-temperature nitrogen adsorption at 77 K on an ASAP 2400 analyzer (Micrometrics, USA).

Palladium (2 wt.%) was deposited on CNTs and 7.3%N–CNT by incipient wetness impregnation using palladium acetate as the palladium precursor. The samples were reduced in 15%H_2/Ar at 200 °C for 1 h [9].

The X-ray photoelectron spectroscopy (XPS) studies were carried out on ES-300 (KRATOS Analytical) and VG ESCALAB HP photoelectron spectrometers with AlK_α radiation. Palladium dispersion in the catalysts was determined by a JEM-2200FS transmission microscope with a resolution of 1 Å.

The CNT and N–CNT diffraction patterns were recorded on a D8 diffractometer (Bruker, Germany) with CuK_α radiation. The sample was placed in a special monocrystalline silicon cuvette cut along the 911 face giving no reflections. The calculated diffraction patterns [10] were obtained using an original model of turbostratically disordered crystals. The model was built as a sequence of a finite number of 2D-periodic layers of graphene and carbon nitride g-C_3N_4 [11]. The disordering was modeled by statistical substitution of graphene layers with g-C_3N_4 layers in 3:1, 1:1, 1:3 ratios, and turbostratic disorder was introduced as random deviations of all layers from their equilibrium positions.

The Raman spectra were recorded on a HORIBA LabRAM HR800 spectrometer equipped with a laser operating at a wavelength of 632.8 nm.

The electrical conductivity of CNTs and N–CNTs at room temperature ($\sigma_{293\,K}$, S/cm) was determined by the standard four-point method.

The water absorption capacity of CNTs and N–CNTs was measured by the gravimetric method. The electrochemical properties of carbon materials were studied by cyclic voltammetry using a symmetrical two-electrode cell and two electrolytes (6M KOH or 1M H_2SO_4).

The catalytic activity of CNTs, N–CNTs, 2%Pd/CNTs, and 2%Pd/N–CNTs in the reaction of oxidative desulfurization of dibenzothiophene (DBT) was measured in a periodic thermostated capacitive quartz reactor. A 25 mg sample with the addition of 20 mL of model fuel (99.5 wt.% $C_{16}H_{34}$ + 0.5 wt.% DBT) was placed in the reactor and heated to 150 °C in a 15 L/h oxygen flow. The reaction time was 6 h. The oxidized fuel was analyzed for total sulfur content on an

ASE-2 energy-dispersive X-ray sulfur analyzer, and the composition of hydrocarbon products was determined on an Agilent 6890N chromatography mass spectrometer.

RESULTS AND DISCUSSION

Physiochemical properties of N–CNTs. The CNTs and N–CNTs were compared by XPS. Fig. 1 shows C1 *s* and O 1*s* spectra of CNTs and 7.3%N–CNTs with the maximum nitrogen doping. The C 1*s* CNT spectrum has a peak at 284.4 eV. This binding energy is characteristic of sp^2 hybridized carbon structures [12]. In the 7.3%N–CNT sample, the C 1*s* peak is shifted by 0.3 eV towards higher binding energies, while the spectrum is broadened in the region of binding energies around 285 eV. A similar change of the C 1*s* spectrum was observed when nitrogen is incorporated into the carbon structure [13-15]. Note however that spectrum broadening above 285 eV may be also due to the presence of various oxygen-containing groups [13]. Indeed, the O 1*s* spectra of CNTs and N–CNTs exhibit a similar set of peaks with binding energies 530.5 eV, 532.1 eV, 533.4 eV, and 535 eV which can be assigned to quinone, carbonyl, phenolic (or carboxyl), and hydroxyl groups, respectively [16-19]. The peak at ~530.5 eV may also be partially related to the oxidized state of iron in the composition of the growth catalyst of CNTs and N–CNTs [20].

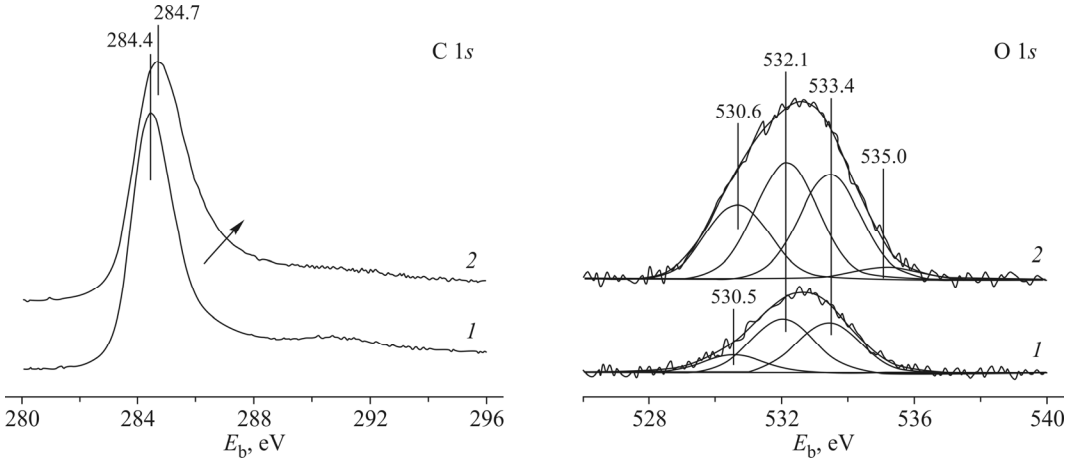

Fig. 1. C 1*s* and O 1*s* spectra of CNTs (*1*) and 7.3%N–CNTs (*2*).

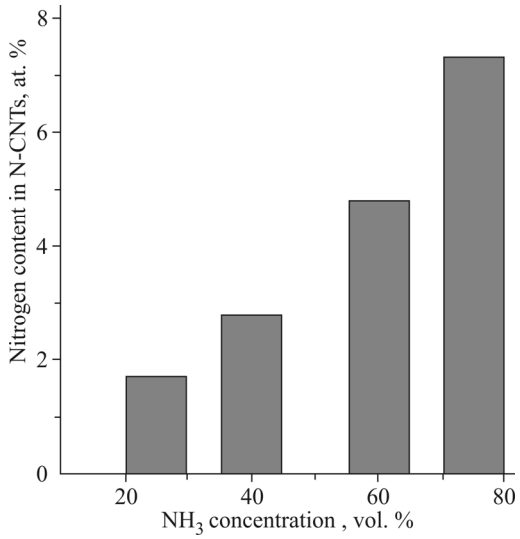

Fig. 2. Nitrogen content in N–CNTs as a function of ammonia concentration in the reaction mixture.

As can be seen in Fig. 2, using a reaction mixture of simple C_2H_4–NH_3 precursors with different component ratios makes it possible to vary the nitrogen content in N–CNTs in the range from 0 at.% to ~7 at.% whereas the degree of doping increases monotonically with ammonia concentration. This is a typical effect of N/C ratio on the nitrogen concentration in N–CNTs. It was also described earlier by other authors when using ammonia and various nitrogen containing organic compounds as the nitrogen source [21-23].

According to the XPS data, nitrogen in N–CNTs is typical of N–CNMs pyridine-like (N_{Py}, ~398 eV), pyrrolic (N_{Pyr}, ~400 eV), graphite-like (N_Q, ~401 eV), oxidized (N_{Ox}, ~402 eV), and molecular (N_{N2}, ~405 eV) states [24]. Note that graphite-like and pyridine-like forms are the predominant ones, but the N_Q content varies within in a narrow range (30-38%) as the total nitrogen content increases, while the N_{Py} content increases from 20% to 43% (Fig. 3). Therefore, varying the reaction mixture composition yields N–CNTs characterized by different (~ 2 times) ratios of main nitrogen forms N_{Py}/N_Q and different main forms. As is known, nitrogen incorporation into the pyridine-like position should be accompanied by the formation of carbon vacancies to compensate the charge, i.e. the defectivity of the structure increases [25, 26].

Decomposition of pure ethylene leads mainly to the formation of multi-walled tubes with an average diameter of 8 nm (Fig. 4). In turn, graphene layers of N–CNTs with an average diameter of 15-17 nm begin to curve and internal arches are formed. It is known that the incorporation of nitrogen into the graphene provokes the layer's curvature [27]. As a result, N–CNTs with a maximum nitrogen content of 7.3 at.% are characterized by a pronounced bamboo-like structure. According to the XPS data, relative contribution of N_{Py} increases with increasing total nitrogen content. Therefore, it can be assumed that the formation of such a structure is associated with pyridine-like nitrogen. Note that all N–CNT samples exhibit some inhomogeneity of the segment length and the number of layers in the arches, apparently, due to different nitrogen content in distinct tubes [28].

In addition to typical reflections of turbostratically disordered graphite-like carbon materials at ~26° (002), ~43° (100), and ~53° (004) [10, 29], the N–CNT diffraction patterns exhibit a superstructural reflection at ~12° (Fig. 5*a*). Note that a similar reflection for N–CNTs was observed in [30], and the N–CNT diffraction pattern reported in [31] contained a number of superstructural reflections characteristic of the hexagonal carbon nitride phase. Evidently, the appearance of the superstructural reflection at ~12° is related to the nitrogen incorporation into the carbon structure, since no such reflection is observed in the CNT diffraction pattern. The analysis of publications showed that the reflection at small angles is a structural reflection for the layered carbon nitride phase g-C_3N_4 due to the formation of structural elements containing four ordered carbon vacancies surrounded by pyridine-like nitrogens (Fig. 5*b*) [32]. The formation of such structural elements increases the intralayer lattice parameter by a factor of 3 (up to 7 Å).

We simulated the N–CNT structure using g-C_3N_4 structural elements. Mixing graphite and carbon nitride layers in different ratios (1:3, 1:1, and 3:1) and introducing turbostratic disordering allowed obtaining diffraction patterns (Fig. 5*b*)

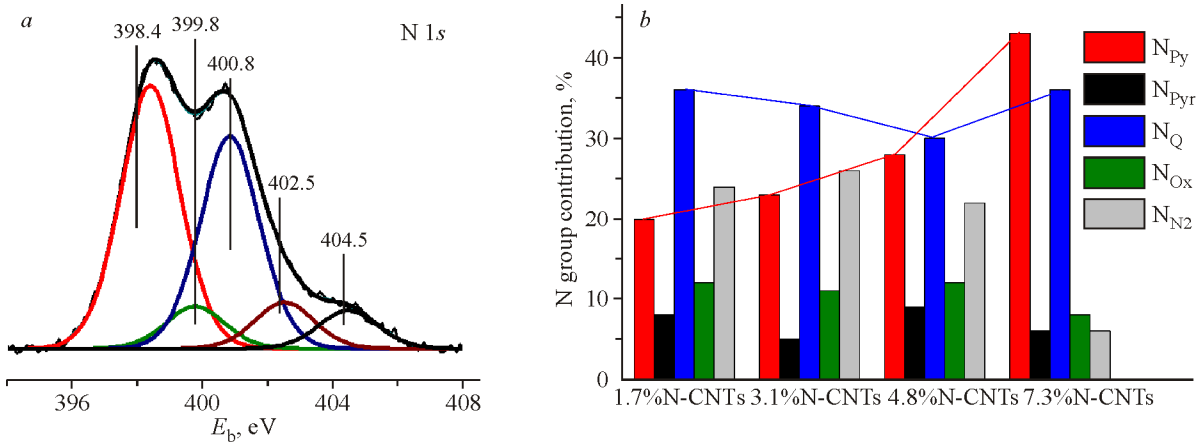

Fig. 3. N 1*s* spectrum of 7.3%N–CNTs (*a*) and contribution of N groups in N–CNTs with various nitrogen contents (*b*).

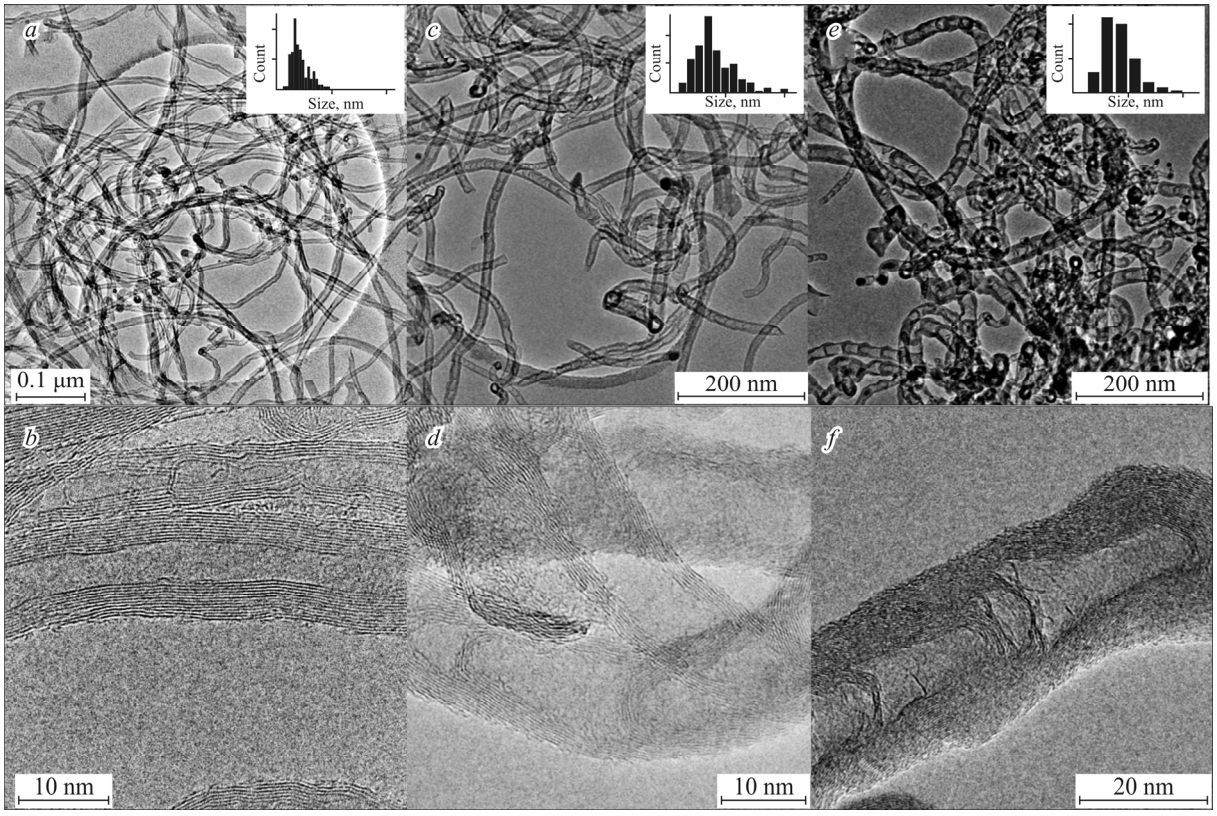

Fig. 4. TEM images of CNTs (*a*, *b*), 1.7%N–CNTs (*c*, *d*), and 7.3%N–CNTs (*e*, *f*).

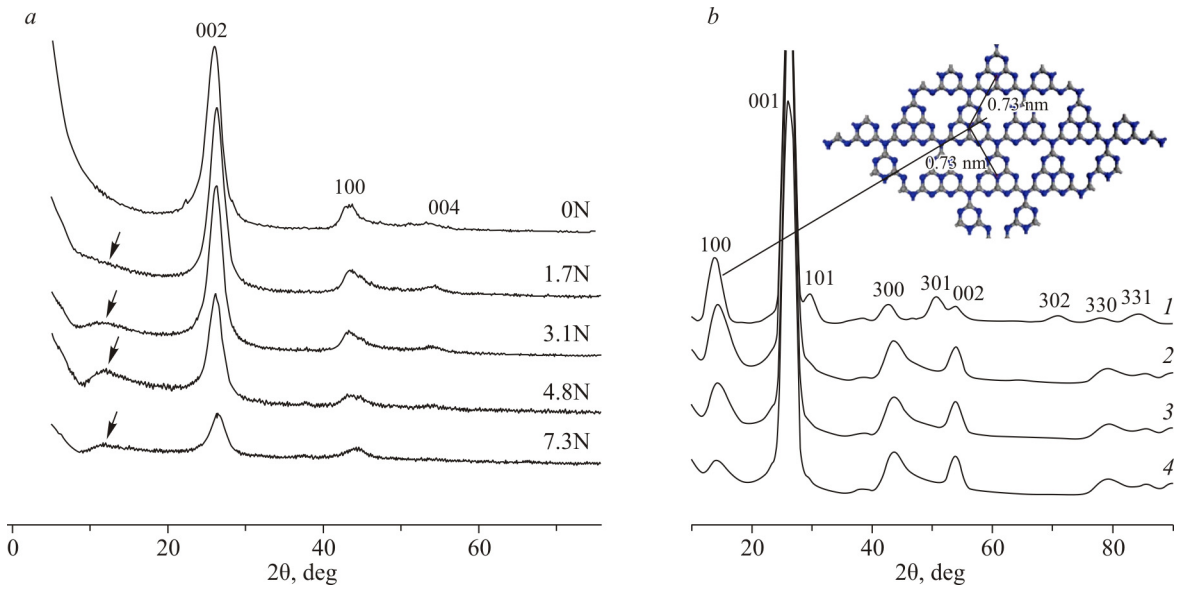

Fig. 5. X-ray diffraction patterns of CNTs and N–CNTs (*a*); calculated diffraction patterns of g-C_3N_4 (*1*), and for the models of turbostratically disordered material consisting of graphene layers and g-C_3N_4 layers in ratios 1:3 (*2*), 1:1 (*3*), and 3:1 (*4*) (*b*). The inset shows a fragment of the g-C_3N_4 layer [33].

similar to the experimental ones (Fig. 5*a*). A good agreement between experimental and calculated diffraction patterns suggests that the N–CNT layer contains fragments of the g-C_3N_4 layer similar to the described ones resulting in an additional peak at small diffraction angles.

A relationship between the N–CNT defectivity and nitrogen content is also confirmed by Raman spectroscopy data showing a monotonic increase of the ratio of the integral intensity of the D and G bands with the degree of doping, while the

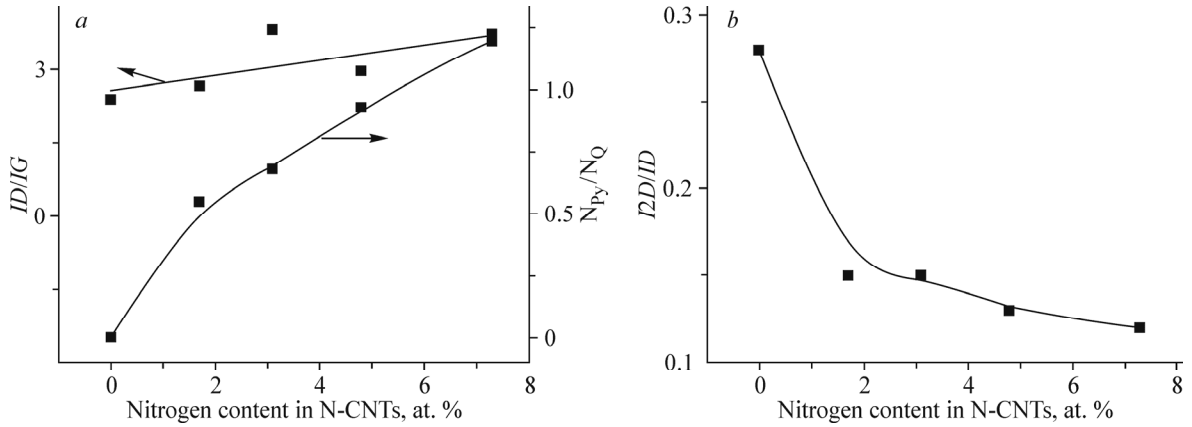

Fig. 6. *ID*/*IG* (*a*) and *I*2*D*/*ID* (*b*) dependences according to Raman spectroscopy data and N_{Py}/N_Q dependence according to XPS data (*a*) plotted as functions of nitrogen content in N–CNTs.

value of this ratio correlates with relative contribution of the pyridine-like nitrogen (Fig. 6). The decrease of the 2D/D ratio also indicates that the size of the defect-free graphene blocks decreases as the nitrogen content in N–CNTs increases [34, 35].

Thus, varying the component ratio in the mixture of simple precursors C_2H_4–NH_3 can be used to easily control the nitrogen content in N–CNTs in the range from 0 at.% to 7.3 at.% and to obtain materials with different nitrogen ratios in graphite-like and pyridine-like states. The increase of nitrogen content in N–CNTs is accompanied by increasing relative contribution of pyridine-like nitrogen and, consequently, the carbon structure defectivity. The XRD data and the performed simulation suggest that graphene layers of N–CNTs contain fragments similar to the structural elements of layer g-C_3N_4, which contain ordered carbon vacancies surrounded by pyridine-like nitrogen. Therefore, the discovered structural features of N–CNTs and the presence of nitrogen centers on the surface are expected to change the functional properties of N–CNTs in various applications compared to those of undoped carbon nanotubes.

Capacitance properties of N–CNTs. As is known, electrical energy in electrochemical supercapacitors is accumulated due to the formation of a electric double-layer on the surface of electrodes (capacitance) and, additionally, due to Faraday redox reactions proceeding on the electrode surfaces involving various surface groups (pseudocapacitance). In the case of N–CNMs, redox reactions in acidic media can proceed with the participation of pyridine-like nitrogen centers [36, 37]. Therefore, the comparative studies of electrochemical properties of CNTs and N–CNTs were performed in alkaline and acidic electrolytes (Fig. 7). The Table 1 lists the obtained values of the total specific capacitance and the

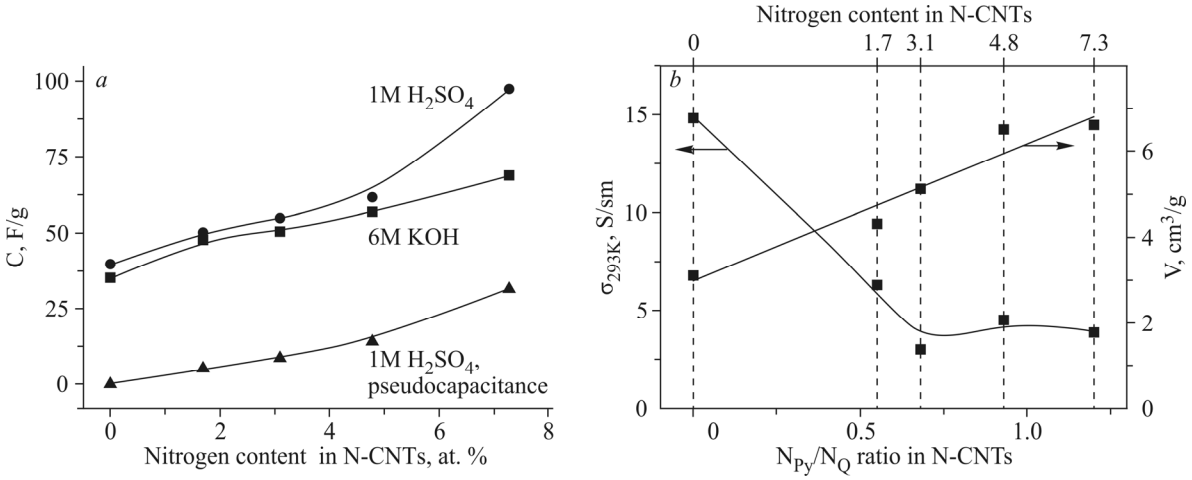

Fig. 7. Specific capacitance of N–CNTs (*C*) as a function of nitrogen content in various electrolytes with a potential sweep rate of 10 mV/s (*a*) and electrical conductivity ($\sigma_{293\,K}$) and water absorption capacity (*V*) as functions of nitrogen content and the N_{Py}/N_Q ratio in N–CNTs (*b*).

TABLE 1. Specific Surface of Samples; O, N_{Py}, and Fe Contents According to XPS Data; Total Specific Capacitance and Specific Pseudocapacitance at Potential Sweep Rates of 10 mV/s and 80 mV/s in an Acidic Electrolyte

Sample	S_{BET}, m^2/g	O, at.%	N_{Py}, at.%	Fe, at.%	Total specific capacitance, F/g		Specific pseudocapacitance, F/g	
					10 mV/s	80 mV/s	10 mV/s	80 mV/s
CNTs	154	1.6	0	0.05	39.3	31.1	0	0
1.7%N–CNTs	155	1.5	0.4	0.10	49.7	40.5	5	4
3.1%N–CNTs	160	2.6	0.6	0.15	54.6	44.4	9	10
4.8%N–CNTs	157	3.7	1.2	0.30	61.2	53.2	14	10
7.3%N–CNTs	151	4.6	2.7	0.55	97.2	82.6	31	28

pseudocapacitance of synthesized materials. In both electrolytes, the total specific capacitance increases together with the doping degree of carbon nanotubes (~2-2.5 times) and a typical [24, 37] capacitance decrease with increasing scanning rate due to diffusion restrictions is observed.

The cyclic voltammetry curves have a shape typical of electric double-layer supercapacitors (Fig. 8). In the case of acidic electrolyte, the N–CNT curves show additional symmetric peaks, referred to as Faraday peaks, appearing as a result of redox reactions. Usually, the fact that the total specific capacitance of N–CNMs is higher than that of CNTs is related to better conductive properties and electrolyte affinity of N–CNMs as well as to the appearance of pseudocapacitance due to nitrogen centers.

Indeed, doping CNMs with nitrogen should increase their electrical conductivity due to the formation of an additional donor state near the Fermi level in the case of graphite-like nitrogen or an additional acceptor state due to the incorporation of nitrogen in pyridinic position resulted in the formation of a carbon vacancy [26]. At the same time, the analysis of reported data shows that the electrical conductivity of N–CNMs can increase [38] or decrease with increasing nitrogen content because of the increased structure defectivity [8, 39]. According to the data shown in Fig. 7*b*, the electrical conductivity of CNTs is 14.8 S/cm, while that of N–CNTs does not exceed 6.3 S/cm. The discovered decrease of the conductivity of N–CNTs is related to their increased defectivity, i.e. the formation of fragments similar to g-C_3N_4 structural elements in the graphene layer. In fact, we showed earlier using synchrotron-radiation XPS with variable analysis depth that pyridine-like nitrogen is incorporated into external and internal graphene layers and into internal arches [40].

On the contrary, doping of CNTs with nitrogen significantly increases the tube's water absorption capacity. The value of this parameter correlates well with the N_{Py}/N_O ratio in N–CNTs and reaches ~6 cm^3/g for 7.3%N–CNTs (Fig. 7*b*). Such a high value suggests that the inner N–CNT channel is filled volumetrically despite multiple inner arches (Fig. 4).

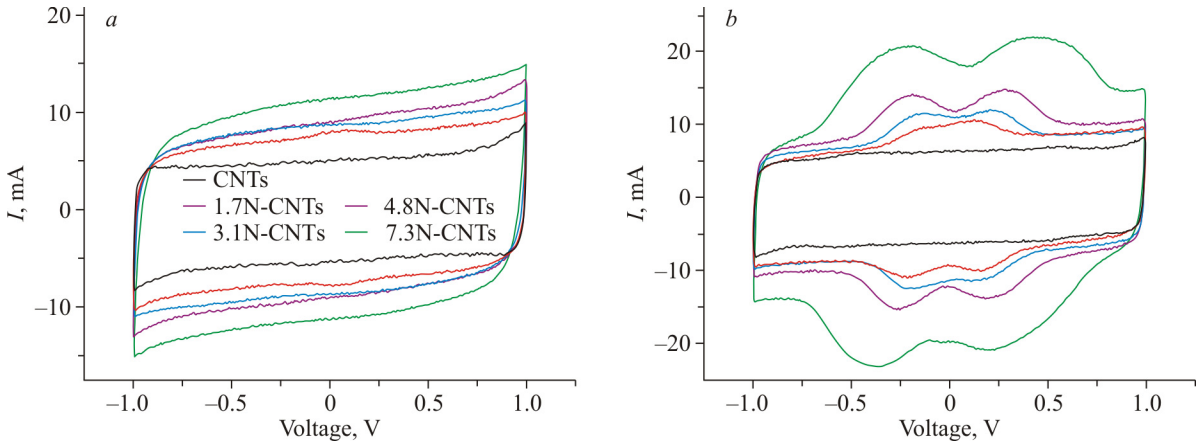

Fig. 8. Cyclic voltammetry curves for CNTs and N–CNTs in alkaline (*a*) and acidic (*b*) electrolytes at a potential sweep rate of 80 mV/s.

Apparently, the presence of large defects (ordered carbon vacancies surrounded by pyridine-like nitrogens) in graphene layers improves the wettability of N–CNTs and makes the capillarity effect more pronounced [22, 41]. Thus, the size of the layer fragment containing four ordered carbon vacancies is at least 5 Å. Hence, improved hydrophilic properties of N–CNTs may be one reason for the increase of the total specific capacitance of N–CNTs compared with that of CNTs in both electrolytes, while different behaviors in alkaline and acidic electrolytes can be explained by the pseudocapacitance effect.

It is known that Faraday processes in acidic media may involve oxygen-containing surface groups [42], nitrogen centers [37], and residual metals of growth catalysts [43]. Indeed, the content of these electrochemically active forms increases together with nitrogen content in N–CNTs (see the Table 1). However, it is unlikely that O-groups and the growth catalyst contribute to the pseudocapacitance of synthesized N–CNTs. According to XPS, the surfaces of CNTs and N–CNTs contain identical acidic and basic O-groups (Fig. 2), and CNTs show no Faraday peaks in both electrolytes. In turn, according to the XRD data, the initial CNT and N–CNT growth catalyst consists of alloy Ni_xFe_y and spinel $[Fe,(Al)]_2O_4$. The XRD registered only phase Ni_xFe_y after the CNT and N-CNT growth. Thus, since the main difference between N–CNTs and CNTs is that the former contain nitrogen (pyridine-like) centers while the compositions of O-groups (according to XPS) and Fe containing growth catalyst (according to XRD) are identical, the pseudocapacitance seems to be mainly caused by pyridine-like centers. As can be seen from the Table 1, the pseudocapacitance contribution increases with increasing N_{Py} content to reach 30% for the 7.3%N–CNT sample.

The maximum specific capacitance for 7.3%N–CNTs in an acidic electrolyte was 100 F/g, which is a high value given low specific surface area of N–CNTs (~150 m^2/g). Note that the obtained results are in good agreement with the data reported for N–CNTs in various electrolytes [24, 44].

N–CNTs as a catalyst and a support for the Pd catalyst. Finally, we compared N–CNTs and CNTs as a catalyst and a support of the palladium catalyst in the reaction of oxidative desulfurization of fuel. The choice of this reaction is due to previously reported data on the catalytic activity of N–CNMs in various oxidation reactions [45-48]. The reaction of oxidative desulfurization of model fuel based on hexadecane with dissolved dibenzothiophene (DBT) has an important application concerning the production of ultra-clean diesel fuels [49]. The main task is to choose the optimal catalyst to remove S-containing sulfur compounds in "soft" conditions without oxidizing the C_{16+} hydrocarbon fuel to oxygenates (ketones, alcohols, organic acids) and deep oxidation products (carbon dioxide and water). The DBT oxidation can be associated with the formation of selective hydrogenolysis products (e.g., biphenyl in the case of DBT) and deep oxidation products (SO_2, CO_2, and H_2O) via the intermediate stage of sulfoxide and/or sulfone formation (Scheme 1).

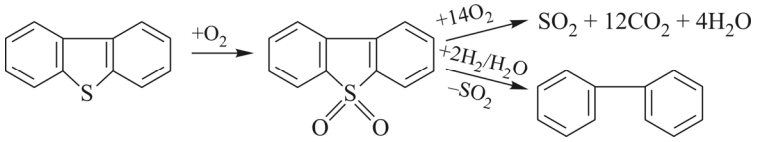

Scheme 1. Oxidation of DBT.

As can be seen from Fig. 9, CNTs and 7.3%N–CNTs show significantly higher reactivity in DBT oxidation (60-80% conversion) than in $C_{16}H_{34}$ oxidation (20-30% conversion), while DBT is oxidized mainly to sulfone. Undoped carbon tubes show higher activity than N–CNTs, possibly due to a stronger adsorption of reagents on N–CNTs containing pyridine-like nitrogen centers on the surface [50]. The decrease of electron transfer in N–CNTs compared to CNTs can be also responsible for the conversion decrease, since the reaction rate on conducting carbon catalysts is facilitated by electron transfer between adsorbed initial reagents, intermediate surface compounds, and final products [51, 52].

To increase the oxidation depth of DBT, palladium in the amount of 2 wt.% was deposited on the CNTs and 7.3%N–CNTs. It was found that palladium indeed increases the DBT conversion. At the same time, the selectivity of deep DBT conversion into SO_2, CO_2, and H_2O and the $C_{16}H_{34}$ conversion to oxygenates increase. Catalyst 2%Pd/7.3%N–CNTs exhibited higher activity and selectivity in deep DBT oxidation than 2%Pd/CNTs, whereas the content of DBT–SO_2 (sulfone)

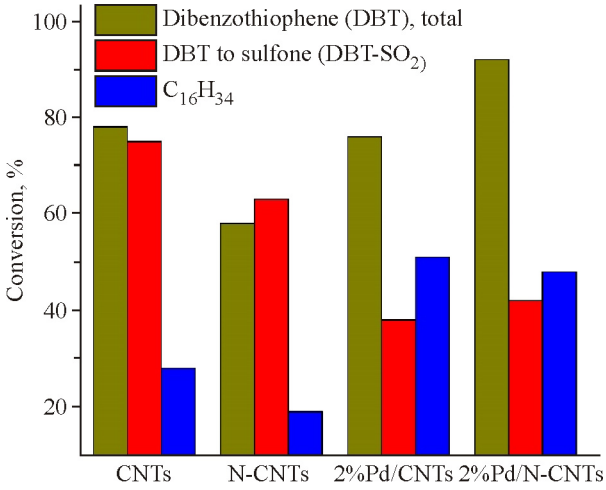

Fig. 9. Activity of CNTs, 7.3%N–CNTs, 2%Pd/CNTs, and 2%Pd/7.3%N–CNTs in the oxidation reaction of the 99.5%$C_{16}H_{34}$–0.5%DBT mixture at 150 °C.

and oxygenates were comparable. Again, the observed facts indicate a higher DBT adsorption on N–CNT nitrogen centers, while high oxidizing ability of Pd-centers seems to promote rapid oxidation of adsorbed DBT and active site regeneration.

It was determined by dark-field microscopy and by XPS that 2%Pd/CNTs contain metallic palladium (E_b (Pd $3d_{5/2}$) = 335.6 eV) in the form of nanoparticles with an average size of 2.6 nm). Catalyst 2%Pd/N–CNTs contains nanoparticles of metallic palladium (E_b (Pd $3d_{5/2}$) = 335.5 eV) with an average size of 1.6 nm and isolated palladium ions (E_b (Pd $3d_{5/2}$) = 337.7 eV) which are formed due to the anchoring on the defects based on pyridine-like nitrogen centers of N–CNMs [4]. Apparently, these differences in palladium dispersion and electronic states explain different activity and selectivity of catalysts in this reaction. It is known that interaction of metals with nitrogen centers of N–CNMs affects their catalytic properties in various reactions, including reactions of complete and selective oxidation [53-56]. The obtained results demonstrate the sensitivity of CNTs/N–CNTs and supported palladium to the reaction of oxidative desulfurization and suggest the need for further research.

CONCLUSIONS

We report a comprehensive study of the properties of bamboo-like N–CNTs prepared by decomposing a simple ethylene-ammonia mixture on a Fe containing catalyst. It was shown that increasing the total nitrogen content in N–CNTs increases the contribution of pyridine-like nitrogen, and fragments similar to g-C_3N_4 structural elements are formed in graphene layers, which leads to a decrease in the electrical conductivity of N-CNTs. On the contrary, the formation of such defects significantly increases the N–CNT affinity to aqueous solutions to enhance their electrochemical activity in alkaline and acidic electrolytes. The maximum specific capacitance of N–CNTs is ~100 F/g in the acidic electrolyte, while the pseudocapacitance contribution, mainly due to pyridine-like nitrogen, reaches 30%. It was shown that the reaction of oxidative desulfurization of fuels can be controlled using carbon nanomaterials with specific surface composition or by adjusting the properties of palladium stabilized on defects with the participation of pyridine-like nitrogen.

ACKNOWLEDGMENTS

The authors acknowledge Dr. Svintsitsky and Dr. Stonkus for some of performed physical and chemical studies.

FUNDING

The synthesis of the samples and the study of their activity in the reaction of oxidative DBT desulfurization were funded by the Russian Science Foundation (project No. 19-13-00129).

CONFLICT OF INTERESTS

The authors declare that they have no conflict of interests.

REFERENCES

1. K. N. Wood, R. O′Hayre, and S. Pylypenko. *Energy Environ. Sci*., **2014**, *7*, 1212.
2. O. Y. Podyacheva and Z. R. Ismagilov. *Catal. Today*, **2015**, *249*, 12.
3. Y. Cao, S. Mao, M. Li, Y. Chen, and Y. Wang. *ACS Catal*., **2017**, *7*, 8090.
4. D. A. Bulushev, M. Zacharska, A. S. Lisitsyn, O. Y. Podyacheva, F. S. Hage, Q. M. Ramasse, U. Bangert, and L. G. Bulusheva. *ACS Catal*., **2016**, *6*, 3442.
5. W. Liu, Y. Chen, H. Qi, L. Zhang, W. Yan, X. Liu, X. Yang, S. Miao, W. Wang, C. Liu, A. Wang, J. Li, and T. Zhang. *Angew. Chem*., *Int. Ed*., **2018**, *57*, 7071.
6. K. Gong, F. Du, Z. Xia, M. Durstock, and L. Dai. *Science*, **2009**, *323*, 760.
7. O. Y. Podyacheva, A. N. Suboch, S. N. Bokova-Sirosh, A. I. Romanenko, L. S. Kibis, E. D. Obraztsova, and V. L. Kuznetsov. *Phys. Status Solidi Basic Res*., **2018**, *255*, 1700253.
8. M. A. Kanygin, O. V. Sedelnikova, I. P. Asanov, L. G. Bulusheva, A. V. Okotrub, P. P. Kuzhir, A. O. Plyushch, S. A. Maksimenko, K. N. Lapko, A. A. Sokol, O. A. Ivashkevich, and P. Lambin. *J. Appl. Phys*., **2013**, *113*, 144315.
9. E. V. Matus, A. N. Suboch, A. S. Lisitsyn, D. A. Svinsitskiy, E. Modin, A. Chuvilin, Z. R. Ismagilov, and O. Y. Podyacheva. *Diamond Relat. Mater*., **2019**, *98*, 107484.
10. S. V. Cherepanova and S. V. Tsybulya. *J. Mol. Catal*., *A*, **2000**, *158*, 263.
11. O. Y. Podyacheva, S. V. Cherepanova, A. I. Romanenko, L. S. Kibis, D. A. Svintsitskiy, A. I. Boronin, O. A. Stonkus, A. N. Suboch, A. V. Puzynin, and Z. R. Ismagilov. *Carbon*, **2017**, *122*, 475.
12. R. Larciprete, S. Gardonio, L. Petaccia, and S. Lizzit. *Carbon*, **2009**, *47*, 2579.
13. T. Susi, T. Pichler, and P. Ayala. *Beilstein J. Nanotechnol*., **2015**, *6*, 177.
14. J. P. Zhao, Z. Y. Chen, T. Yano, T. Ooie, M. Yoneda, and J. Sakakibara. *Appl. Phys. A*, **2001**, *73*, 97.
15. R. Droppa, P. Hammer, A. C. M. Carvalho, M. C. dos Santos, and F. Alvarez. *J. Non. Cryst. Solids*, **2002**, *299–302*, 874.
16. R. Larciprete, P. Lacovig, S. Gardonio, A. Baraldi, and S. Lizzit. *J. Phys. Chem. C*, **2012**, *116*, 9900.
17. K.F. Ortega, R. Arrigo, B. Frank, R. Schlogl, and A. Trunschke. *Chem. Mater*., **2016**, *28*, 6826.
18. J. H. Zhou, Z. J. Sui, J. Zhu, P. Li, D. Chen, Y. C. Dai, and W. K. Yuan. *Carbon*, **2007**, *45*, 785.
19. P. Burg, P. Fydrych, D. Cagniant, G. Nanse, J. Bimer, and A. Jankowska. *Carbon*, **2002**, *40*, 1521.
20. E.Paparazzo. *J. Electron Spectrosc. Relat. Phenom*., **1987**, *43*, 97.
21. X. Y. Tao, X. B. Zhang, F. Y. Sun, J. P. Cheng, F. Liu, and Z. Q. Luo. *Diamond Relat. Mater*., **2007**, *16*, 425.
22. K. Chizari, I. Janowska, M. Houlle, I. Florea, O. Ersen, T. Romero, P. Bernhardt, M. J. Ledoux, and C. Pham-Huu. *Appl. Catal. A*, **2010**, *380*, 72.
23. L. G. Bulusheva, A. V. Okotrub, Y. V. Fedoseeva, A. G. Kurenya, I. P. Asanov, O. Y. Vilkov, A. A. Koos, and N. Grobert. *Phys. Chem. Chem. Phys*., **2015**, *17*, 23741.
24. E. V. Lobiak, V. R. Kuznetsova, A. A. Makarova, A. V. Okotrub, and L. G. Bulusheva. *Mater. Chem. Phys*., **2020**, *255*, 123563.
25. M. Terrones, P. M. Ajayan, F. Banhart, X. Blase, D. L. Carroll, J. C. Charlier, R. Czerw, B. Foley, N. Grobert, R. Kamalakaran, P. Kohler-Redlich, M. Rühle, T. Seeger, and H. Terrones. *Appl. Phys. A*, **2002**, *74*, 355.
26. C. P. Ewels and M. Glerup. *J. Nanosci. Nanotechnol*., **2005**, *5*, 1345.
27. W. Q. Han, P. Kohler-Redlich, T. Seeger, F. Ernst, and M. Rühle. *Appl. Phys. Lett*., **2000**, *77*, 1807.
28. R. J. Nicholls, Z. Aslam, M. C. Sarahan, A. M. Sanchez, F. Dillon, A. A. Koos, P. D. Nellist, and N. Grobert. *Phys. Chem. Chem. Phys*., **2015**, *17*, 2137.

29. I. V. Mishakov, Y. I. Bauman, Yu. V. Shubin, L.S. Kibis, E.Y. Gerasimov, M.S. Mel′dinov, V.O. Stoyanovskii, S.V. Korenev, and A.A. Vedyagin. *Catal. Today*, **2020**, https://doi.org/10.1016/j.cattod.2020.06.024.
30. R. Chetty, S. Kundu, W. Xia, M. Bron, W. Schuhmann, V. Chirila, W. Brandl, T. Reinecke, and M. Muhler. *Electrochim. Acta*, **2009**, *54*, 4208.
31. A. G. Kudashov, A. V. Okotrub, L. G. Bulusheva, I. P. Asanov, Yu. V. Shubin, N. F. Yudanov, L. I. Yudanova, V. S. Danilovich, and O. G. Abrosimov. *J. Phys. Chem. B*, **2004**, *108*, 9048.
32. G. Liao, S. Chen, X. Quan, H. Yu, and H. Zhao. *J. Mater. Chem*., **2012**, *22*, 2721.
33. M. J. Bojdys, J. O. Müller, M. Antonietti, and A. Thomas. *Chem. Eur. J*., **2008**, *14*, 8177.
34. R. Podila, J. Chacón-Torres, J. T. Spear, T. Pichler, P. Ayala, and A. M. Rao. *Appl. Phys. Lett*., **2012**, *101*, 123108.
35. D. V. Krasnikov, S. N. Bokova-Sirosh, T. O. Tsendsuren, A. I. Romanenko, E. D. Obraztsova, V. A. Volodin, and V. L. Kuznetsov. *Phys. Status Solidi B*, **2018**, *255*, 1700255.
36. Y. Deng, Y. Xie, K. Zoua, and X. Ji. *J. Mater. Chem. A*, **2016**, *4*, 1144.
37. Y. H. Lee, K. H. Chang, and C. C. Hu. *J. Power Sources*, **2013**, *227*, 300.
38. I. Kunadian, S. M. Lipka, C. R. Swartz, D. Qian, and R. Andrews. *J. Electrochem. Soc*., **2009**, *156*, K110.
39. Z. R. Ismagilov, A. E. Shalagina, O. Yu. Podyacheva, A. V. Ischenko, L. S. Kibis, A. I. Boronin, Y. A. Chesalov, D. I. Kochubey, A. I. Romanenko, O. B. Anikeeva, T. I. Buryakov, and E. N. Tkachev. *Carbon*, **2009**, *47*, 1922.
40. D. A. Svintsitskiy, L. S. Kibis, D. A. Smirnov, A. N. Suboch, O. A. Stonkus, O. Y. Podyacheva, A. I. Boronin, and Z. R. Ismagilov. *Appl. Surf. Sci*., **2018**, *435*, 1273.
41. K. V. Kumar, K. Preuss, Z. X. Guo, and M. M. Titirici. *J. Phys. Chem. C*, **2016**, *120*, 18167.
42. Y. J. Oh, J. J. Yoo, Y. I. Kim, J. K. Yoon, H. N. Yoon, J. H. Kim, S. B. Park, and Y. Joon. *Electrochim. Acta*, **2014**, *116*, 118.
43. E. O. Fedorovskaya, L. G. Bulusheva, A. G. Kurenya, I. P. Asanov, and N. A. Rudina. *Electrochim. Acta*, **2014**, *139*, 165.
44. Y. Zhang, C. Liu, B. Wen, X. Song, and T. Li. *Mater. Lett*., **2011**, *65*, 49.
45. Y. Gao, G. Hu, J. Zhong, Z. Shi, Y. Zhu, D. S. Su, J. Wang, X. Bao, and D. Ma. *Angew. Chem*., *Int. Ed*., **2013**, *52*, 2109.
46. Y. Lin, X. Pan, W. Qi, B. Zhang, and D. S. Su. *J. Mater. Chem. A*, **2014**, *2*, 12475.
47. C. Chen, J. Zhang, B. Zhang, C. Yu, F. Peng, and D. Su. *Chem. Commun*., **2013**, *49*, 8151.
48. K. Chizari, A. Deneuve, O. Ersen, I. Florea, Y. Liu, D. Edouard, I. Janowska, D. Begin, and C. Pham-Huu. *ChemSusChem*, **2012**, *5*, 102–108.
49. Z. Ismagilov, S. Yashnik, M. Kerzhentsev, V. Parmon, A. Bourane, F. M. Al-Shahrani, A. A. Hajji, and O. R. Koseoglu. *Catal. Rev.: Sci. Eng*., **2011**, *53*, 199.
50. G. Yang, H. Chen, H. Qin, and Y. Feng. *Appl. Surf. Sci*., **2014**, *293*, 299.
51. K. Ohkubo, H. Kitaguchi, and S. Fukuzumi. *J. Phys. Chem. A*, **2006**, *110*, 11613.
52. J. Luo, F. Peng, H. Wang, and H. Yu. *Catal. Commun*., **2013**, *39*, 44.
53. X. Ning, H. Yu, F. Peng, and H. Wang. *J. Catal*., **2015**, *325*, 136.
54. X. Ning, Y. Li, B. Dong, H. Wang, H. Yu, F. Peng, and Y. Yang. *J. Catal*., **2017**, *348*, 100.
55. A. B. Ayusheev, O. P. Taran, I. A. Seryak, O. Yu. Podyacheva, C. Descorme, M. Besson, L. S. Kibis, A. I. Boronin, A. I. Romanenko, Z. R. Ismagilov, and V. Parmon. *Appl. Catal. B*, **2014**, *146*, 177.
56. O. Y. Podyacheva, Z. R. Ismagilov, A. I. Boronin, L. S. Kibis, E. M. Slavinskaya, A. S. Noskov, N. V. Shikina, V. A. Ushakov, and A. V. Ischenko. *Catal. Today*, **2012**, *186*, 42.